JMEPEG
https://doi.org/10.1007/s11665-024-10265-4

1059-9495/$19.00

ORIGINAL RESEARCH ARTICLE

Low-Temperature Sintering of Colloidal Gold Nanoparticles by Salt Addition

L. Catanzaro, V. Scardaci, M. Scuderi, M. Condorelli, L. D'Urso, and G. Compagnini

Submitted: 16 February 2024 / Revised: 19 May 2024 / Accepted: 17 June 2024

Gold nanoparticles synthetized by pulsed laser ablation in liquid with a mean diameter of 4 nm were joined together by adding potassium bromide solution at various concentrations. By increasing the salt concentration, there is a significant increase of the particle size up to a mean diameter of 18 nm. We have studied the nanoparticle merging by using atomic force and electron microscopy characterizations, also demonstrating that it is possible to deposit sintered nanoparticles on silanized substrates in a fast, simple, cost-effective, energy-saving method with relevance in industrial manufacturing.

Keywords electronic materials, joining, low-temperature sintering, metal nanoparticles, nanojoining, nanomaterials, salt

1. Introduction

Sintered metal nanoparticles (NPs) have played a crucial role in electronic device applications, especially as electrodes or circuits. Notably, gold (Au) and silver (Ag) NPs are the best choice due to their exceptional conductivity, robust resistance against oxidation and considerable stability (Ref 1, 2, 3, 4).

Classical sintering methods for ceramics and metals require processing at high temperatures, close to their melting temperature, in order to induce the atomic movement between interfaces (Ref 5). Achieving high temperatures make processes highly energy and time consuming; thus, the discovery of new low-temperature, low-cost and environmentally friendly sintering processes is of primary importance nowadays (Ref 6, 7, 8). The use of metal NPs, instead of bulk materials, is a good strategy to reduce the sintering temperature, as their large surface area, compared to volume, makes them less stable than bulk (Ref 9, 10). However, this is not sufficient to substantially reduce the energy consumption.

New efficient sintering methods allowing process temperature reduction include laser sintering, electrical sintering, photonic sintering, etc… (Ref 7, 11, 12, 13)

Physical sintering methods typically require expensive equipment and high-energy consumption, while chemical sintering processes are capable of joining metal NPs at room temperature by only using wet chemistry (Ref 1, 4, 14, 15).

Generally, the first steps of NP sintering involve the formation of a neck between NPs which leads to physical contact and, gradually, the coalescence of the particles themselves which, at the end, provokes the formation of a continuous percolated network (Ref 13).

In the literature, there are some examples of chemical sintering of metal NPs in which the removal of a stabilizer polymer from the surface of Ag NPs and the addition of a polycation solution lead to the merging among NPs due to their destabilization (Ref 16). This method uses polymers which may not be a perfect solution for high-temperature electronic devices because of their degradation temperature.

Sintering chemical agents used for Ag NPs could also be halides (Ref 4, 8, 17). What is required here is an interaction, between NPs and a fusion agent, that is stronger than NP capping agent as is shown in the work of Magdassi et al. (Ref 15), where Ag NP sintering is obtained through the addition of sodium chloride solution which is able to replace their capping agents.

Moreover, it is well known that the addition of halide salts to Au NPs causes the fusion of NP themselves due to the displacement of the stabilizer (Ref 18, 19, 20).

In our earlier investigation, we focused the attention on the parameters which control NP aggregation induced by salt solutions (Ref 21). Here we studied the sintering of Au NPs obtained by pulsed laser ablation in a chloride salt solution and joined by using very low concentrations of a potassium bromide (KBr) solution, which are then deposited onto silicon substrates. We characterized sintered NPs by using UV–Vis spectroscopy, supported by numerical simulations, as well as microscope techniques like scanning electron transmission microscopy (STEM) and atomic force microscopy (AFM).

In literature, most of the works were made by using capped Au NPs, synthetized by chemical synthesis methods and

This article is an invited paper selected from abstracts submitted to the 5th International Conference on Nanojoining and Microjoining (NMJ 2023), held from November 27 to 29, 2023, in Leipzig, Germany. It has been expanded from the original presentation. The issue was organized by Dr. Susan Hausner, TU Chemnitz and Jolanta Janczak-Rusch, EMPA.

L. Catanzaro, V. Scardaci, and **L. D'Urso**, Dipartimento di Scienze Chimiche, Università degli Studi di Catania, Catania, Italy; **M. Scuderi**, CNR–IMM, Strada VIII n.5 Zona Industriale, 95121 Catania, Italy; **M. Condorelli** and **G. Compagnini**, Dipartimento di Scienze Chimiche, Università degli Studi di Catania, Catania, Italy; and Istituto Nazionale Scienza e Tecnologia dei Materiali (INSTM), Catania, Italy. Contact e-mails: Lucrezia.catanzaro@phd.unict.it and vittorio.scardaci@unict.it.

Published online: 15 October 2024

sintered with higher concentrations of salt (Ref 18, 19, 20), while, in our work, the Au NPs prepared by laser are "naked," a characteristic which eliminates the usual physical contact issues associated with capped NPs and it helps to reduce the salt concentration.

2. Materials and Methods

Gold colloid is obtained by pulsed laser ablation in liquid (PLAL) with the fundamental frequency of a Nd:YAG laser (Quanta system) which was focused by a lens (focal length 10 cm) onto a gold target immersed in 10mM solution of sodium chloride at pH=9. The laser with a fluence of 0.6-1J/cm^2 had a repetition rate of 10Hz and a pulse width of 5ns.

UV–Vis measurements were made by using an Agilent Cary 60 spectrometer. Finite-difference-time-domain (FDTD) simulations, through Lumerical software package, were used to simulate the plasmon resonance spectra of Au NPs.

STEM micrographs were made by using a probe Cs-corrected JEM-ARM200F by JEOL with a primary beam energy of 200 keV and a high-angle annular dark-field detector. In order to make STEM measurements, the NPs were dropped out from the solution by using a lacey-carbon STEM grid. The ImageJ software was used to obtain NP size distributions.

Substrates for AFM imaging were initially cleaned and hydroxylated through a piranha treatment (H_2O_2/H_2SO_4) and, then, silane functionalized by immersing them in 1% (3-Aminopropyl)triethoxysilane (APTES) solution (Ref 22). Then the substrates were immersed in gold colloid for 2 hours.

3. Results and Discussion

It is well known that the salt addition provokes the colloidal aggregation (Ref 2, 23, 24), as is shown in Fig. 1 where the plasmon resonance spectrum of a gold colloid changes after addition of salt. In Fig. 1 we report the plasmon resonance spectra of a gold colloid almost 30 minutes after the addition of different quantities of salt achieving a final concentration ranging from 25 to 35mM KBr.

The change of the surface plasmon resonance (SPR) compared to the as-prepared one is an indication of an aggregation phenomenon which starts in presence of KBr (Ref 25, 26, 27). The SPR spectra obtained after almost 30 minutes of adding KBr show two plasmon resonance bands, the one at the lowest wavelength, close to the original one, named transversal surface plasmon resonance (T-SPR) band, while the other at the highest wavelength is known as longitudinal surface plasmon resonance (L-SPR) band (Ref 21, 21).

It is interesting to note the redshift of the original SPR mode after the addition of KBr (Fig. 1), which, according to literature, could be associated to different factors such as the formation of Au-Br or Au-OH bonds on NP's surface that could change the local environmental refractive index (Ref 18) or an increase of NP's size (Ref 28, 29). The refractive index change is too low to justify such a huge redshift, while the latter hypothesis is more realistic.

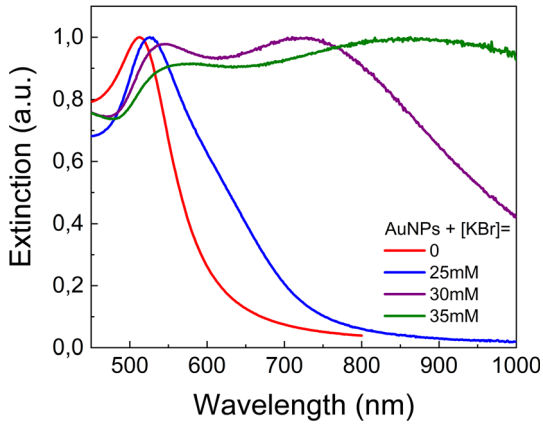

Fig. 1 Normalized SPR spectra of Au NPs before and after the addition of 25, 30 and 35mM of potassium bromide solution

In order to support such hypothesis, we simulated the SPR spectra of short linear aggregates made of 5 gold NPs with a gap of 0.5nm and NP size ranging from 10 to 20nm. In Fig. 2a, we show the evolution of the T-SPR peak by increasing NPs size, and in Fig. 2b, we report their T-SPR shift compared to the experimental T-SPR shift. The increase of NP size leads to a redshift of the T-SPR peak; even if the simulated redshift is very low compared to the experimental shift, they both have an exponential trend. The mismatch between experimental and simulated data could be associated with the aggregation behavior, since the aggregates may not be completely linear, which could influence the T-SPR position (Ref 28).

Figure 3 shows STEM images of Au NPs before (Fig. 3a) and after the addition of various concentrations of KBr (Fig. 3b, c and d). At a first glance, Au NPs in presence of higher quantities of salt are less spherical than the as-prepared ones. From a systematic analysis of STEM images, we established the NP size distributions before and after salt addition, as discussed below.

The analysis of gold NP size distribution in colloid (Fig. 4) reveals an increase of NP size, starting from a mean diameter of 4±1nm and reaching 18±5nm after the addition of the highest quantities of salt. The correlation between NP size and salt concentration is evident in Fig. 3b to d and in NP size distribution graphs from Fig. 4b to d. By focusing the attention on the NP size distribution at each salt concentration, we can propose the occurrence of an Ostwald ripening and merging effects between NPs. Comparing the mean diameter and the standard deviation of NP size distribution in presence of the lowest concentration of KBr (Fig. 4b) with the as-prepared gold colloid (Fig. 4a), we can hypothesize an Ostwald ripening effect where bigger NPs grow at the expense of smaller ones.

In Fig. 4c ([KBr] = 30 mM), we observe two NP distributions, the first one has a mean diameter ($\overline{d_1} = 10 \pm 3$nm) resembling the one obtained in 25 mM of KBr and the second one ($\overline{d_2} = 20 \pm 2$nm) similar to the one in presence of 35 mM of KBr. Likely, between 25 and 35 mM of KBr, NP growth is influenced by a coalescence effect among NPs with a mean diameter of 10 nm, resulting in the formation of NP with an average diameter of 20 nm.

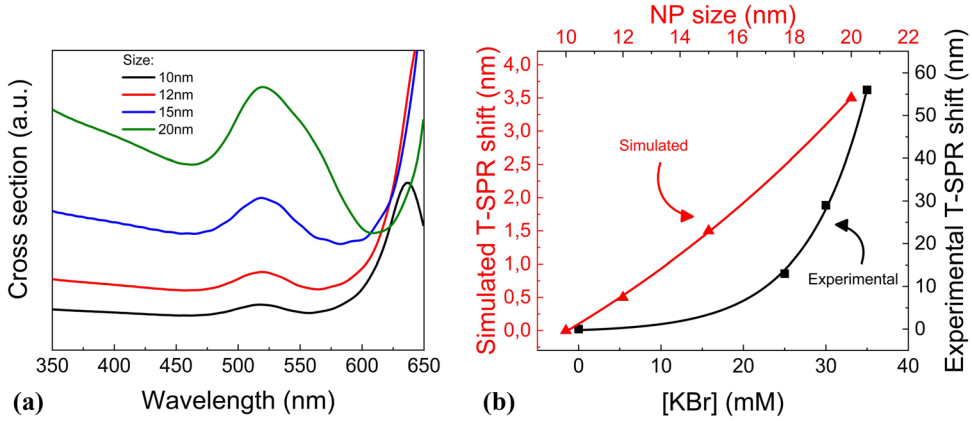

Fig. 2 (a) Simulated SPR spectra of linear aggregates made of 5 gold NPs with a gap of 0.5nm and a size ranging from 10 to 20nm. (b) Comparison between experimental and simulated T-SPR shift

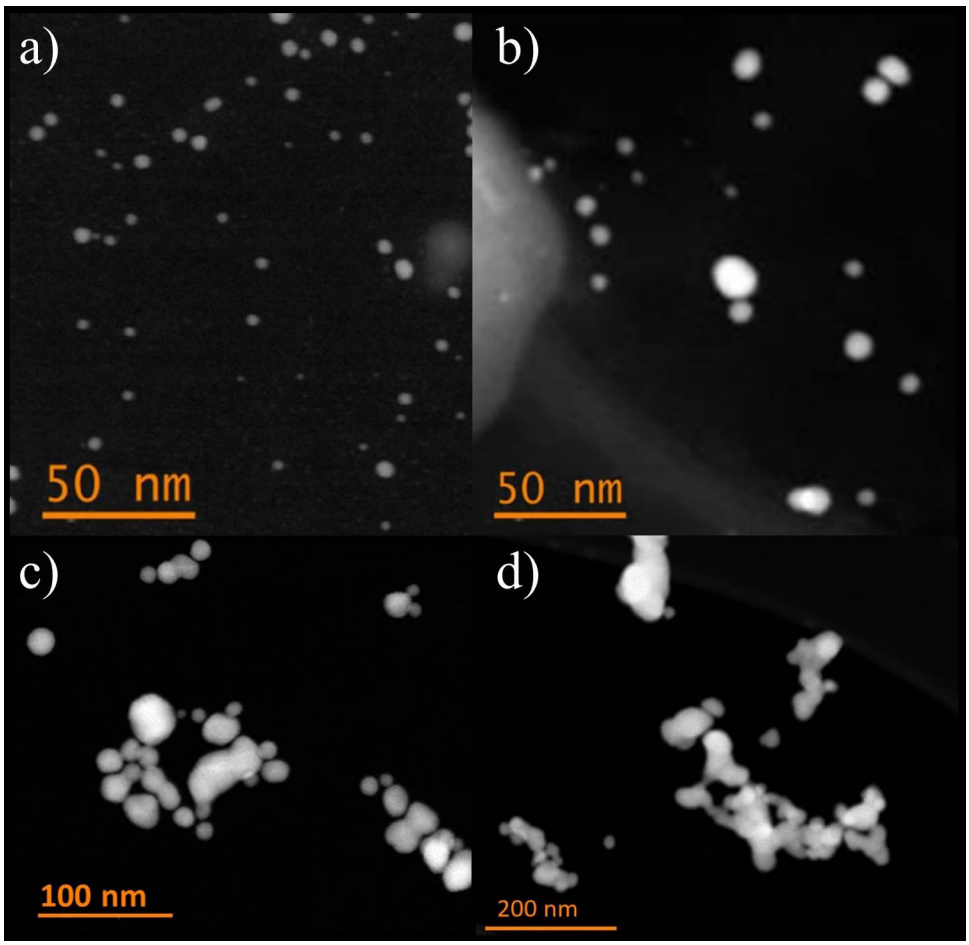

Fig. 3 STEM images of Au NPs (a) before and after the addition of (b) 25, (c) 30 and (d) 35mM of KBr

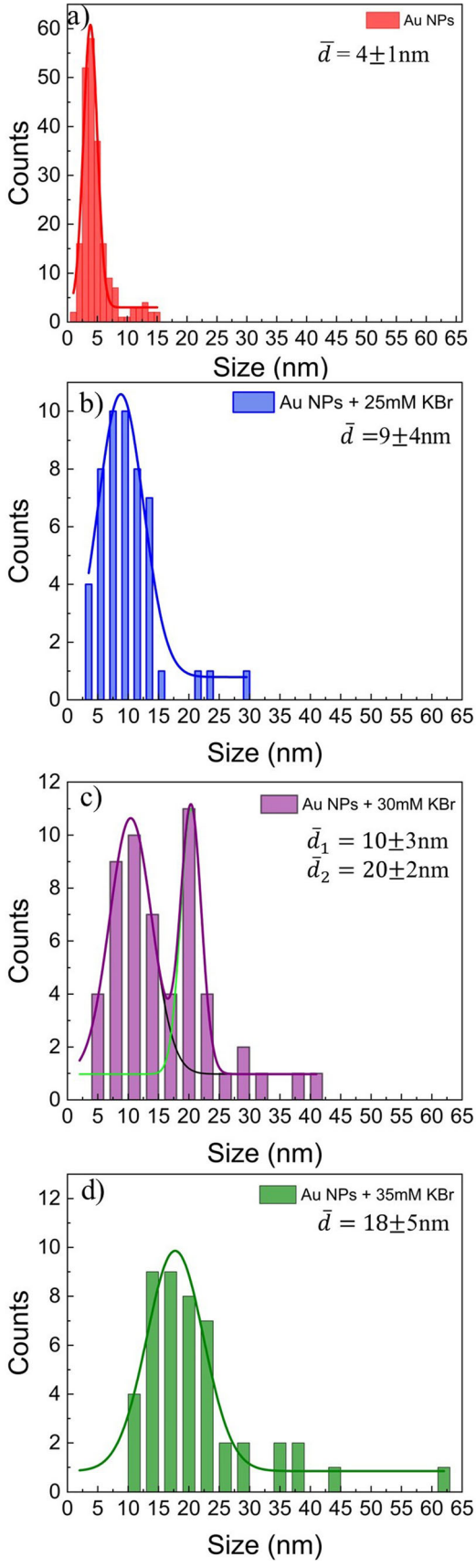

Fig. 4 Gaussian fits of NP size distributions estimated by measuring the diameter of NPs from STEM images (a) before and after the addition of (b) 25, (c) 30 and (d) 35mM of salt

The effect of bromide on Au NPs capped with glutamic acid was reported by Guo et al. (Ref 20) where they show that a NaBr solution starting from a concentration of 50 mM provokes the slight increase of NPs size. They hypothesized that the increasing of NP collision induced by the salt would lead to NP fusion through an Ostwald ripening phenomenon, because the bromide, thanks to its high affinity with gold, is able to bind to the NP surface by displacing the capping agents. In our case, the Au NPs are stable thanks to the chemisorption of the chloride, but the higher affinity of Br^- compared to Cl^- likely causes the displacement of the "stabilizer" provoking NP fusion at very low concentration.

Figure 5a shows the evidence of interconnections between NPs after adding salt. In particular, the two NPs are bonded together with the formation of the classical fusion neck which could be seen as the initial phase of NP melting.

Figure 5b shows another example of gold aggregates obtained with the highest quantities of salt, in which Au NPs were totally joined together forming percolation pathways. It is clear that for these types of samples it is difficult to estimate the NP size due to the increase of the neck size, which is strictly correlated with salt concentration, but we can observe, without any doubt, the increase in NP size.

After studying the behavior of Au NPs in presence of salt, we transferred gold aggregates onto silicon substrates. Figure 6 shows AFM images of the deposited Au NPs with the related cross sections.

The as-prepared NPs have a section of almost 6-7nm which agrees with the NP size distribution estimated with STEM images. After the addition of salt, the cross section of Au NPs starts growing with a height of almost 25, 60 and 600 nm, respectively, for 25, 30 and 35mM of KBr. The cause of such huge increase of the height is likely the out of plane NP agglomeration. Overall, there is a clear growth trend of NPs aggregates by increasing salt concentration. The results obtained at the highest KBr concentration (35mM) show a remarkable interconnection between NPs, forming a percolating network on silicon substrates, which is of key importance for sintering-based industrial processes looking to make metal interconnections.

4. Conclusions

In this work, we explore the room temperature sintering process of Au NPs induced by different concentrations of a potassium bromide solution. The Au NPs, prepared by laser ablation, undergo sintering by adding very low concentrations of salt (from 25 to 35mM). The crucial effects induced by the halide were investigated by STEM images which reveal the growth of NPs from 4nm up to 18nm. Based on our observations, we hypothesize that the NP growth is the result of the simultaneous presence of two key effects: Ostwald ripening and coalescence. The latter seems to be prevalent with higher concentrations of salt. Then, aggregates were successfully deposited onto silicon substrates, laying the fundamental basis for potential application in electronic devices.

The innovative sintering method not only provides a cost-effective and energy-efficient solution but also contributes to reduce sintering time, making it promising for industrial applications.

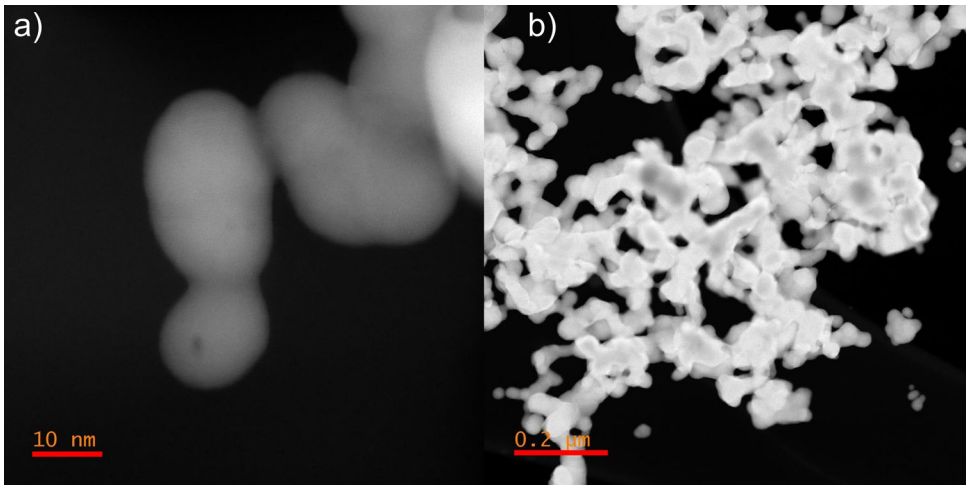

Fig. 5 (a) Evidence of merging effect between NPs with the formation of the characteristic neck between sintered particles. (b) STEM images of interconnected gold NPs obtained in presence of 35mM of KBr

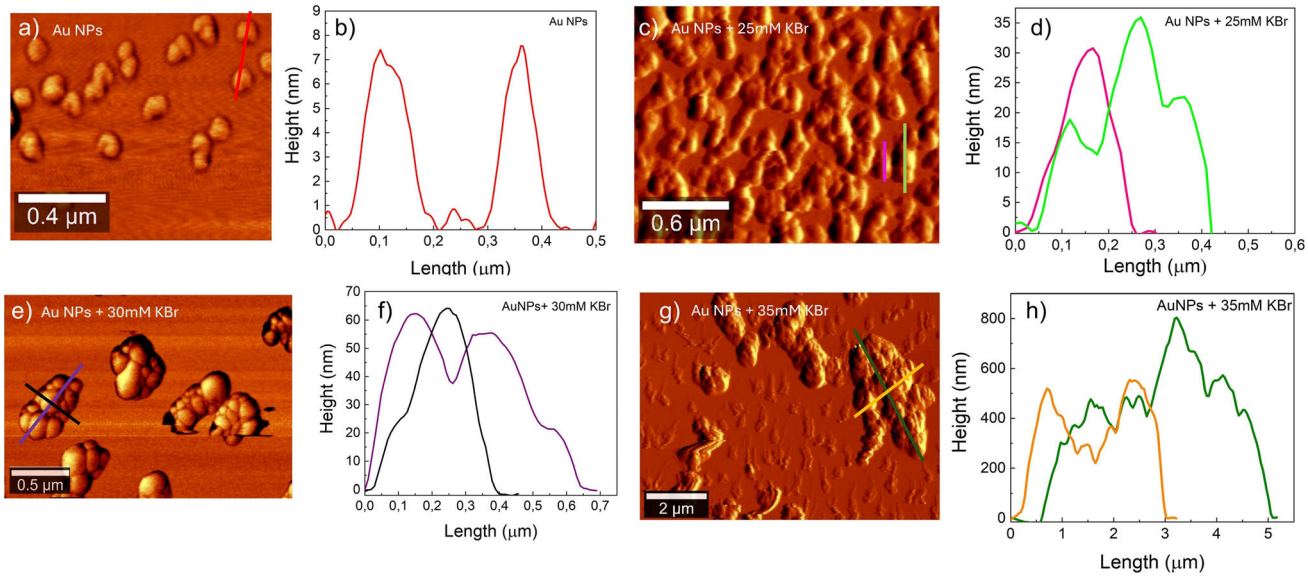

Fig. 6 Respectively, AFM images and cross section analysis of (a, b) isolated and aggregated Au NPs after the addition of (c, d) 25 (e, f) 30 and (g, h) 35mM of salt

Potentially, based on the theoretical explanation of the sintering mechanism which lies behind our halogen chemically induced sintering method, we should be able to apply this sintering method to any colloid containing very small metal NPs weakly capped with a great affinity to halogen ions.

Acknowledgments

The author V.S. wishes to acknowledge funding and support by European Union (NextGenerationEU), through the MUR-PNRR project SAMOTHRACE (ECS00000022). The authors L. C., L. D., G. C., gratefully acknowledge PRIN 2022 PNRR ELATED. PON Innovazione e Green DM 1062 is acknowledged by M.C. This work was supported by PON project Bionanotech Research and Innovation Tower (BRIT) financed by the Italian Ministry for Education.

Funding

Open access funding provided by Università degli Studi di Catania within the CRUI-CARE Agreement.

Open Access

References

1. P. Peng et al., Room-Temperature Joining of Silver Nanoparticles Using Potassium Chloride Solution for Flexible Electrode Application, *J. Phys. Chem. C*, 2018, **122**, p 2704–2711.
2. D. He, J. Yang, J. Zhang and C. Hu, Salt-induced Nanoporous Gold Electrodes: One-step Scalable Fabrication of High-performance Flexible Electrochemical Sensors from Gold Nanoparticles, *Sensors Act. B Chem.*, 2023, **396**, 134559
3. W. Cui et al., Gold Nanoparticle Ink Suitable for Electric-Conductive Pattern Fabrication Using in Ink-jet Printing Technology, *Colloids Surfaces A Physicochem. Eng. Asp.*, 2010, **358**, p 35–41.
4. B.F.Y. Rezaga and M.D.L. Balela, Chemical Sintering of Ag Nanoparticle Conductive Inks at Room Temperature for Printable Electronics, *J. Mater. Sci. Mater. Electron.*, 2021, **32**, p 17764–17779.
5. K. Lu, Sintering of nanoceramics, *Int. Mater. Rev.*, 2008, **53**, p 21–38.
6. X. Kuang, G. Carotenuto and L. Nicolais, Review of Ceramic Sintering and Suggestions on Reducing Sintering Temperatures, *Adv. Perform. Mater.*, 1997, **4**, p 257–274.
7. Kravchuk, O., Lesyuk, R., Bobitski, Y. & Reichenberger, M. Sintering methods of inkjet-printed silver nanoparticle layers. in *Springer Proceedings in Physics* vol. 210 317–339 (Springer Science and Business Media, LLC, 2018)
8. Zapka, W., Voit, W., Loderer, C. & Lang, P. Low temperature chemical post-treatment of inkjet printed nano-particle silver inks. in *International Conference on Digital Printing Technologies* 906–911 (2008). https://doi.org/10.2352/issn.2169-4451.2008.24.1.art00115_2
9. J. Awayes, I. Reinkensmeier, G. Wagner and S. Hausner, Nanojoining with Ni Nanoparticles for Turbine Applications, *J. Mater. Eng. Perform.*, 2021, **30**, p 3178–3186.
10. D. Deng, Y. Jin, Y. Cheng, T. Qi and F. Xiao, Copper Nanoparticles: Aqueous Phase Synthesis and Conductive Films Fabrication at Low Sintering Temperature, *ACS Appl. Mater. Interfaces*, 2013, **5**, p 3839–3846.
11. J. Noh, J. Ha and D. Kim, Femtosecond and Nanosecond Laser Sintering of Silver Nanoparticles on a Flexible Substrate, *Appl. Surf. Sci.*, 2020, **511**, 145574
12. M. Hummelgård, R. Zhang, H.E. Nilsson and H. Olin, Electrical Sintering of Silver Nanoparticle Ink Studied by In-situ TEM Probing, *PLoS ONE*, 2011, **6**, e17209
13. L. Mo et al., Silver Nanoparticles Based Ink with Moderate Sintering in Flexible and Printed Electronics, *Int. J. Mol. Sci.*, 2019, **20**(9), p 2124.
14. Y. Tang, W. He, S. Wang, Z. Tao and L. Cheng, New Insight into the Size-Controlled Synthesis of Silver Nanoparticles and its Superiority in Room Temperature Sintering, *CrystEngComm*, 2014, **16**, p 4431.
15. M. Grouchko, A. Kamyshny, C.F. Mihailescu, D.F. Anghel and S. Magdassi, Conductive Inks with a 'Built-in' Mechanism that Enables Sintering at Room Temperature, *ACS Nano*, 2011, **5**, p 3354–3359.
16. S. Magdassi, M. Grouchko, O. Berezin and A. Kamyshny, Triggering the Sintering of Silver Nanoparticles at Room Temperature, *ACS Nano*, 2010, **4**, p 1943–1948.
17. M. Layani and S. Magdassi, Flexible Transparent Conductive Coatings by Combining Self-Assembly with Sintering of Silver Nanoparticles Performed at Room Temperature, *J. Mater. Chem.*, 2011, **21**, p 15378–15382.
18. Z. Zhang et al., Investigation of Halide-Induced Aggregation of Au Nanoparticles into Spongelike Gold, *Langmuir*, 2014, **30**, p 2648–2659.
19. W. Cheng, S. Dong and E. Wang, Iodine-Induced Gold-Nanoparticle Fusion/Fragmentation/Aggregation and Iodine-Linked Nanostructured Assemblies on a Glass Substrate, *Angew. Chem. Int. Ed.. Chem. Int. Ed.*, 2003, **42**, p 449–452.
20. Y. Liu, L. Liu and R. Guo, Br–induced Facile Fabrication of Spongelike Gold/Amino Acid Nanocomposites and Their Applications in Surface-Enhanced Raman Scattering, *Langmuir*, 2010, **26**, p 13479–13485.
21. L. Catanzaro et al., Surface Plasmon Resonance of Gold Nanoparticle Aggregates Induced by Halide Ions, *Mater. Chem. Phys.*, 2023, **308**, 128245
22. R.R. Bhat and J. Genzer, Tuning the Number Density of Nanoparticles by Multivariant Tailoring of Attachment Points on Flat Substrates, *Nanotechnology*, 2007, **18**, 025301
23. D. Wang, B. Tejerina, I. Lagzi, B. Kowalczyk and B.A. Grzybowski, Bridging Interactions and Selective Nanoparticle Aggregation Mediated by Monovalent Cations, *ACS Nano*, 2011, **5**, p 530–536.
24. Zhang, W. *Nanoparticle aggregation: principles and modeling. Advances in experimental medicine and biology* vol. 811 (Adv Exp Med Biol, 2014)
25. R. Pamies et al., Aggregation Behaviour of Gold Nanoparticles in Saline Aqueous Media, *J. Nanoparticle Res.*, 2014, **16**, p 1–11.
26. M. Sun et al., Salt-induced Aggregation of Gold Nanoparticles for Photoacoustic Imaging and Photothermal Therapy of Cancer, *Nanoscale*, 2016, **8**, p 4452–4457.
27. A. Mclean et al., Au Nanobead Chains with Tunable Plasmon Resonance and Intense Optical Scattering: Scalable Green Synthesis, Monte Carlo Assembly Kinetics, Discrete Dipole Approximation Modeling, and Nano-Biophotonic Application, *Chem. Mater.*, 2021, **33**, p 2913–2928.
28. S.K. Ghosh, A. Pal, S. Kundu, S. Nath and T. Pal, Fluorescence Quenching of 1-Methylaminopyrene near Gold Nanoparticles: Size Regime Dependence of the Small Metallic particles, *Chem. Phys. Lett.*, 2004, **395**, p 366–372.
29. K. Esashika, R. Ishii, S. Tokihiro and T. Saiki, Simple and Rapid Method for Homogeneous Dimer Formation of Gold Nanoparticles in a Bulk Suspension based on Van der Waals Interactions Between Alkyl Chains, *Opt. Mater. Express*, 2019, **9**, p 1667.